Numerical simulation of thermal degradations in a high performance concrete test-slab under fire conditions

E. Ouedraogo [1], S. Djaknoun [2], H. Bensalem[1,2], R. Bouchendouka[2]

[1] Univ. Grenoble Alpes, Grenoble INP, Laboratoire 3SR, 38000 Grenoble, France.
Evariste.Ouedraogo@3sr-grenoble-fr

[2] USTHB, Laboratoire de Mécanique Avancée, Alger, Algérie.
sdjaknoun@usthb.dz

Résumé :

Cette étude traite de la modélisation numérique de l'écaillage thermique des bétons visant à évaluer la cohérence des résultats calculés avec les mesures et les observations expérimentales réalisées. Une dalle d'essai en béton à hautes performances équipée de thermocouples a ensuite été soumise à un essai d'écaillage sous un feu un peu plus intense que celui de la norme ISO 834 et au cours duquel l'écaillage s'est produit. L'essai d'écaillage thermique a ensuite été modélisé simultanément en thermique transitoire non linéaire pour déterminer le champ de température et avec un modèle d'endommagement isotrope pour déterminer les champs de contraintes et d'endommagement dans l'éprouvette. L'évolution de la température tout au long de l'essai, mesurée par un thermocouple situé dans la face chauffée de l'éprouvette, a été utilisée pour appliquer des conditions de température imposée sur la face chauffée lors de la modélisation. Les champs de température, de contraintes et d'endommagement et leur évolution en fonction du temps dans des nœuds sélectionnés ont été décrits. La comparaison des températures calculées avec celles mesurées par les thermocouples s'est révélée très satisfaisante. Par conséquent, le champ d'endommagement calculé semble réaliste et suffisamment cohérent avec les observations expérimentales.

Abstract:

This study deals with numerical modelling of spalling aimed at evaluating the consistency of the computed results with the experimental measurements and observations. A high performance concrete test-slab equipped with thermocouples was then subjected to spalling test under a little more severe fire than standard ISO 834 one and during which spalling occurred. The spalling test was then modelled simultaneously in non-linear transient thermal to determine the temperature field and with an isotropic damage model to determine stresses and damage fields in the specimen. The evolution of the temperature all along the test measured by a thermocouple located in the heated face of the specimen was used to apply imposed temperature conditions on the heated face during the modelling. The temperature, stresses and damage fields and their evolution at selected nodes with respect to time are reported. The comparison of the computed temperatures with those measured by the

thermocouples was very satisfactory. Hence the computed damage field seemed realistic and consistent enough with the experimental observations.

Mots clefs: spalling, spalling tests, ISO 834 fire, high performance concrete, thermal modelling, thermomechanical modelling, damage, damage modelling,

1 Introduction

Thermal spalling of concrete is a complex phenomenon currently under research interest because of the rise of high performance concrete, less porous than ordinary concrete and more sensitive to spalling. Spalling are thermal instabilities that occur in concrete subjected to temperature that leads to a loss of matter in surface or in volume. In the literature a lot of studies tried to understand the causes of occurrence, the influencing parameters and how to prevent it essentially by experimental approach [1-5]. A few of them deal with modelling spalling, because of the complexity of the phenomenon [6-7].

In the present study, thermomechanical approach of the phenomenon is considered. Hence a spalling bench test was first designed and fabricated and a test was undertaken on a high performance concrete slab-specimen equipped with temperature sensors. During the test, spalling occurred. The test was then numerically modelled with isotropic damage constitutive equations in non-linear transient thermal. As the applied thermal cycle was time dependent, the dependency of thermo-physical and mechanical characteristics of the material with temperature was taken into account. The evolutions of concrete thermo-physical characteristics with temperature proposed by Eurocode 2 were used. As far as the mechanical characteristics are concerned, data proposed in a paper to be submitted were used [8]. It was then possible to model the spalling test in very good conditions and to obtain realistic results.

In this paper information about the material and operational test conditions are first presented. Then, the experimental results acquired, especially the temperature recorded from the thermocouples are reported. The third part deals with the numerical modelling. A large placed is reserved to thermal modelling which is essential because the damage calculation will be based on it. In the last part before conclusion, temperature, stresses and damage fields and evolutions are then reported and discussed.

2 Materials and properties

The studied material is a high performance concrete which formulation is based on normalized sand. It is constituted of 0-2 mm normalized sand of the Sociéte Nouvelle du Littoral, cement CEM 1 52.5 produced by Vicat, silica fume Condensil SD95 produced by Condensil Company, superplasticizer Sika Viscocrete Tempo 10 produced by Sika and tap water. The W/C ratio was 0.19.

The various constituents of the material were mixed according to a specified protocol and cast. The molds are constituted of the assembly of Plexiglas and steel walls and measure 250x250x100 (mm). The fresh concrete was put in the molds and vibrated during 1 min 30s in two steps. In order to measure the temperature at selected points of the specimen, some thermocouples, placed along the specimen thickness, were embedded in them during the casting. In the specimen studied here, three thermocouples were placed: first on the specimen heated face, second at 10 mm and third at 20 mm. The thermocouples locations are displayed in Fig.1. After the vibration process, the molds were

covered with a plastic film during 24 hours and then demolded. Hence, the cast specimens were squared slabs with 250 mm in length and 100 mm in thickness equipped with K type thermocouples.
In order to widely study spalling phenomenon, an original test bench was designed and fabricated. It consists of a 32 KW power burner associated with a ceramic structure forming then a sort of furnace. The burner was designed so that it heats uniformly the specimen large face. The ceramic structure is constituted of vertical walls which one of them is equipped of a porthole where a camera can be placed to film the test, and an upper horizontal slab pierced with a central hole and peripheral holes. The peripheral holes are aimed at evacuating the burned gas. The central squared hole measures 245x245 in mm and faces the burner; the specimen was placed at the top of the furnace and was then heated through this hole. Another independent type K thermocouple was also placed in the furnace beside the regulation thermocouple of the control unit in order to measure the temperature in the furnace.
During the spalling test, the three embedded thermocouples and the independent thermocouple placed in the furnace were connected to an independent data acquisition system that acquires the data all along the spalling tests. The global view of the apparatus is displayed in Fig.2.

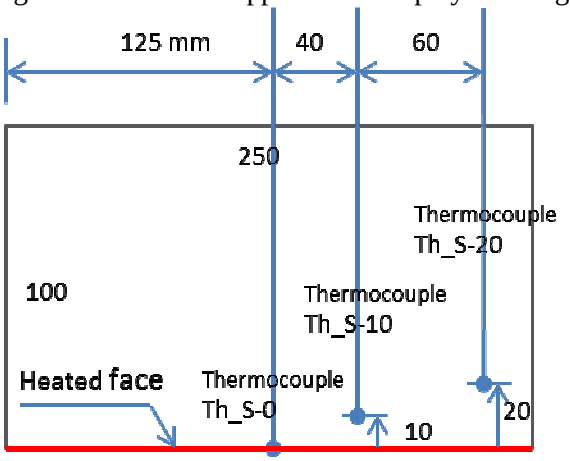

Fig.1. Schematic view of the symmetry plane of the specimen displaying the location of the thermocouples.

a b

Fig.2. Photo of a- a global view of the spalling test bench and b- a detailed view of the specimen equipped with the three thermocouples.

3 Experimental study

The test consisted in placing the instrumented specimen on the furnace once the burner reached it minimum power after the starting regime ended. During the test, the burner power was increased manually in order to obtain a heating rate close to the ISO 834 standard curve. The evolutions of the

various acquired temperatures with respect to time were displayed in real time thanks to data acquisition software. Occurring events such as noise or explosion were collected during the test. Some photos of water coming out of the lateral or upper faces of the specimen were taken and dated. Thermal spalling occurred during the test.

In Fig.3 are displayed the response of the thermocouple located in the furnace (TH_Furn), the responses of those embedded in the specimen at various distances to the heated face (Th_S0, TH_S10, TH_20) and the fire standard ISO 834 curve of Eurocode 2 (TH_ISO834). Globally, the responses of all the thermocouples increased with increasing time. This study covers the ten first min of the spalling test (600 s). The evolution with respect to time of TH_Furn is higher at any time than the curve Th_ISO834 indicating then a more severe applied thermal cycle than the recommended standard. It also presents sudden increase (at times 75 and 310 s) corresponding to the sudden increase of the power that was controlled manually. The evolution of the temperature recorded by the thermocouple which tip was located in the burned face of the specimen is quite different in intensity from the temperature in the furnace but presented the same discontinuities. The difference of intensity is due to the influence of the thermal inertia of the concrete surrounding the thermocouple. A sudden decrease of the temperature was observed at time 490 s. It was the consequence of the occurrence of very noisy thermal spalling. At this time, the furnace temperature TH_Furn decreased from 857 to 737 °C whereas the one of TH_S0 decreased from 424 to 358 °C. That was not the first time that the thermal spalling occurred in the specimen but it was the first time it impacts visibly the thermocouples records. This is probably due to a reduction of burner power consequence the projection of concrete splinters on it. But the zone surrounding the TH_S0 was not affected by the spalling and that's why its temperature decreased. Temperature of the thermocouple located at 10 mm from the heated face (TH_S10) increased regularly with increasing temperature and seemed not affected by the effects of power sudden increases at time 310 s as the previous ones but was slightly affected by the power sudden decrease at time 490 s. The thermocouple located at 20 mm (TH_S20) behaved as the previous one but at lower temperatures logically.

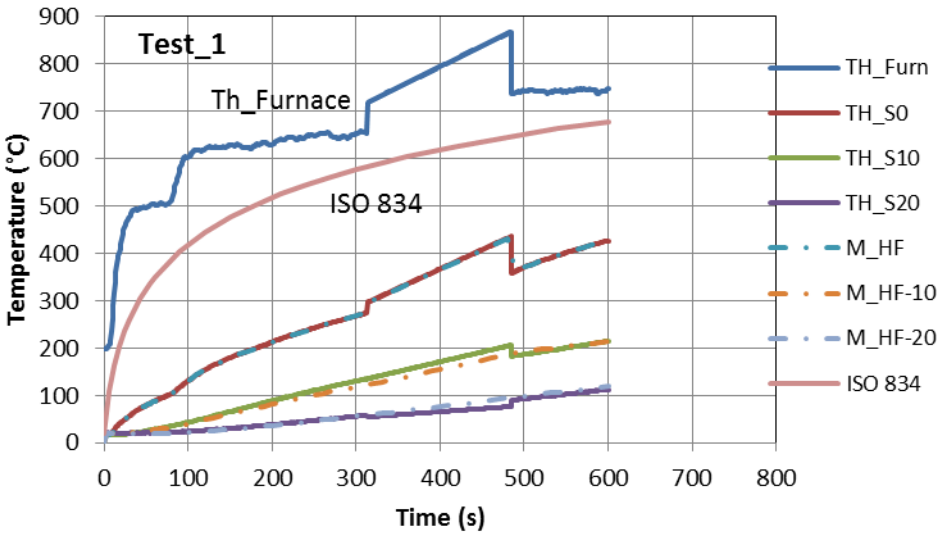

Fig.4. Comparison of the results of modeling of the thermal behavior of specimen 1 considering the modified conductivity curve with experimental results. The modeling was satisfactorily improved.

During the spalling test, post-mortem observations showed that spalling occurred uniformly on the heated face of the specimen what mean that the test bench is adequate. The splinters ejected during the

tests had various shapes and various masses. The ones which mass exceeded 4 g were considered and their dimensions measured. It was then found that their thickness ranged from 5 to 12 mm.

4 Thermo-mechanical study

4.1 Modelling of the thermal field

The aim of the study now is to model the thermal behavior the slabs specimen during the spalling tests reported previously. The specimen has a parallelepipedal shape with the width equal to the length and is uniformly burned on one of its large face. A 3D modelling is a priori convenient. Thanks to the two present symmetry planes and the uniformity of the thermal loading, the study of a fourth of the specimen is representative of the whole specimen. Then one fourth of the specimen was kept to define the finite element model. Hence this model had six faces where some thermal conditions were applied: the upper face that is heated, the lower face in contact with the air, the two symmetry faces where symmetry conditions should be applied and two remaining free faces in contact with the air (Fig.5).

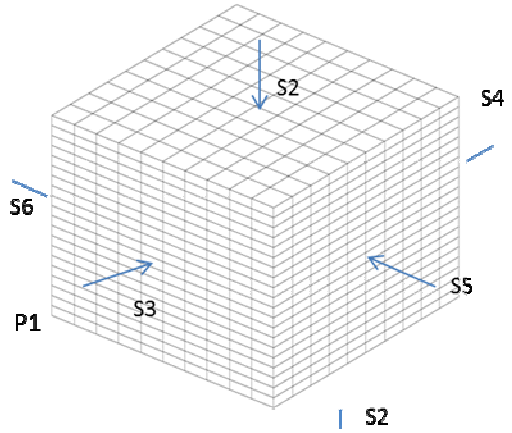

Fig.5. Definition of the areas where boundary conditions are applied on the finite elements model.

The burner heated the specimen through its face and the mode of heat transfer inside the specimen is the conduction governed by Fourier heat equation. This equation can be established from the first principle of thermodynamics and its general form is as following:

$$div\left(\alpha \overrightarrow{grad}T\right) - \rho C_p \left(\frac{\partial T}{\partial t}\right) = -P \qquad (1)$$

Where ρ is the material density, α is the material thermal conductivity, C_P the material specific mass and P the calorific power of the internal sources. In the case where the thermo-physical characteristics of the material depend on the temperature, it takes the following form:

$$\alpha(T)\Delta T + \frac{d\alpha}{dT}\left(\overrightarrow{grad}T\right)^2 - \rho(T)C_p(T)\left(\frac{\partial T}{\partial t}\right) = -P \qquad (2)$$

These last equations were used in the present study since the temperature field varied between 20 and 500°C a range where the thermo-physical characteristics varied significantly. No interne sources were present so P equaled 0.

The temperature field at any point of the studied domain characterized by its geometrical coordinates x depend on time and can be written T(x,t).

The initial conditions were imposed at any point of the studied domain were:

$$T(x,0) = T_i \quad (3)$$

where T_i is the initial temperature, generally set at 20°C.

Boundary conditions are defined on the various faces of the model. First the large free face (A1 in Fig.5) and the lateral free faces (A3 and A6 in Fig.5) of the specimen in contact with air were subjected to convection governed by the following equation:

$$\varphi = H_v(T(M_i,t) - T_{ext}) \quad (4)$$

Where φ is the exchange flux density, H_v is the heat exchange coefficient, $T(M_i,t)$ is the temperature at any point M_i of the considered surfaces and T_{ext} is ambient temperature generally set at 20°C. As the other thermo-physical characteristics, H_v a priori depends on temperature and this should be encountered.
As to the two symmetry faces of the finite model (A4 and A5 in Fig.5), they are not subjected to any exchange and are characterized by adiabatic conditions (no heat transfer).
Lastly the second large face (A2 in Fig.5) of the finite element model is the loading face and was subjected to a imposed-temperature loading. The formulation defining the loading condition is:

$$T(M_i,t) = TH\_S0(t) \quad (5)$$

Where TH_S0 is the temperature measured by the thermocouple located at the burned face of the specimen during the spalling test. The imposed-temperature condition was applied to the upper face in thermal modelling in order to obtain a better view when displaying the temperature field in the specimen, contrary to the experience where the lower face was heated.
The material thermo-physical characteristic and their evolution with respect to temperature were taken from the Eurocode 2: between 20 and 800°C, the density decreased from 2300 to 2185 $kg.m^{-3}$, the specific mass increased from 900 to 1100 $J.kg^{-1}.K^{-1}$ and the thermal conductivity of the material decreased from 1.95 to 0,724 $Wm^{-1}K^{-1}$, respectively. During this study, the thermal exchange coefficient H_v was kept constant at 20 $W.m^{-2}.K^{-1}$.
The finite element code CAST3M developed by CEA-SACLAY in France was used for thermomechanical modelling in transient nonlinear thermal. Cubic quadratic 3D finite elements (CU20) were used to mesh the model. The finite element model was discretized by 10 divisions in the length and the width and 20 divisions in the height. This generated element size of 12.5 mm in length and width and 5 mm in height. Some calculations that were undertaken showed that reducing the length and width of finite elements doesn't affect significantly the thermal behavior but affect considerably the computing time. That's why the current mesh was used. This mesh was designed so that any location of the thermocouples in the specimen matches with a node of the mesh. Hence the comparison of numerical and experimental results was done on the base of coincident geometric points. Hence along the specimen height, a node is present every 5 mm.
In the present study impose-temperature thermal loading was adopted since experimental investigations allowed the measurement of the heated face of the specimen. The evolution with respect to time of the heating face temperature measured by thermocouple TH_S0 will be the imposed-temperature during the numerical finite elements modelling. That was one of the goal of the design and fabrication of the test bench.

4.2 Modelling of the material damage

The thermomechanical numerical modelling of the spalling test was based on the isotropic damage model proposed by Mazars [9]. In the present study the elasticity modulus of the material as the specific model parameters depended on temperature. We performed various tests in compression and in bending conditions at various temperatures on which results the model parameters were identified. These results are reported in a paper that will be submitted soon [10].

5 Results and discussion

5.1 Modelling the thermocouples temperature

A previous study [8] on the same spalling test reported the protocol used in order to obtain the thermal modelling results displayed in Figure Fig.4. In this figure, the modelled curves M_HF-XX are quasi superimposed with the experimental ones TH_SXX. The discrepancy considered in this study is the difference (Th_SXX - M_HF-XX) at a given time. The discrepancies observed at the node located at 10 mm to the heated face at times 200, 440 and 600 were: -6, -15 and -1.5 °C. At the node located at 20 mm to the heated face, at the same times the discrepancies were: -1.7, 11 and 4 °C. The results of the calculations were quite satisfactory and then the computed temperature field was realistic. The computations with the isotropic damage model permitted access to stresses and damage fields.

5.2 Temperature stresses and damage

Fig.6 displays the temperature field in the left column and damage field in the right column at steps 60, 120 and 150 corresponding to times 200, 490 and 600 s, respectively. However the time, the temperature field seems to depend only on the Z axis. The temperature gradient is important at zones close to the heated face of the specimen. The distance to the heated face for which the temperature exceeds 50°C is three finite elements thickness at time 200 s, four finite elements thickness at time 490 s and five finite elements thickness at time 600 s. The longer the time, the deeper the heat penetrates the material. It is also clear that the temperature decreased when the distance to the heated face increased, logically. When examining the damage evolution, it first appeared at the central point located in the heated face and then, at the high corners of the symmetry planes and last, at some of the points located in the heated face. But very quickly it appeared in the inner layers where it reached its maximum values. Considering Fig.6, at any of the times chosen the damage evolved between its minimum value 0 and its maximum value 1. The distribution of damage is interesting. The maximum damage does not develop in the heated face but at one to two to three elements thickness to it. This means that the weakest zones are not located on the heated plane but at planes located deeper. The corners located in the symmetry planes seem more affected by damage than the corner belonging to the lateral faces of the specimen subjected to convection. Hence damage seems to likely occur at zones located in the vicinity of the symmetry planes of the specimen rather than at its corners.

In order to better understand the damage field, investigations on the spatial distribution of normal stresses and the damage along the central z-axis were undertaken and the curves displayed in Fig.7 and 8. Fig.7 displays the spatial distribution of the normal x stresses at nodes located between 0 to 40 mm to the heated face at various loading times: 50, 100, 150, 200, 250, 300, 350, 400, 450, 500, 550, and 600 s. The distance step used to display the spatial distribution was 5 mm, the size of a finite element along the specimen height (node 1 to node 9 in Fig. 5). The curves revealed that the stress distribution is complex enough and that it evolves significantly with thermal loading time. Hence, the node located

in the heated face (node 1) is almost always subjected to compression stresses at moderate levels ranging from 0 to -3.2 MPa.

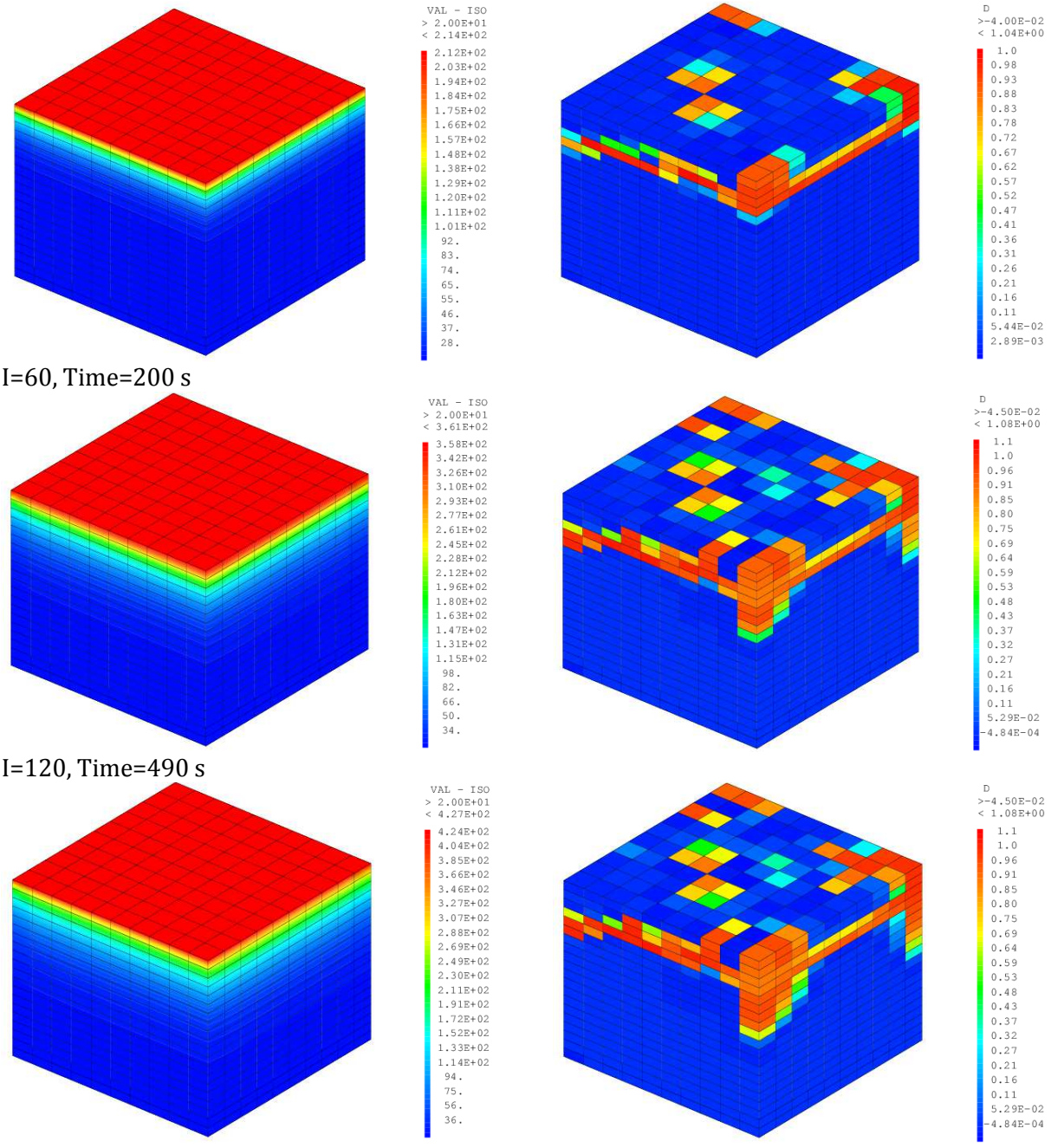

Fig. 6. Temperature (left) and damage (right) distributions in the specimen according to numerical modelling at three loading times: 200, 490 and 600 s.

Another remarkable observation is that the state of stress of node 2 located at d=5 mm is almost of tensile type however the loading time except at 600 s where weak compression stresses were recorded. Between times 0 and 100 s, the spatial distribution stresses reduced (between -1 and +1 MPa). Between times 150 and 250 s, all the layers from 0 to 25 mm (nodes 3 to 5) are subjected to intense tensile stresses which maximum values are: 1.8 MPa at node 5 (d=20 mm) at time 150, 5.5 MPa at node 4 (d=20 mm) at time 200s, and a maximum value of 10 MPa at node 4 (d=15mm) at time 250. Times 300 to 350 appears as transition time in the evolution of the spatial distribution. By time 400 up to 600s, layer near the heated face (nodes 1 to 3) are in compression whereas layers far from the

heated face are in tension the limit point being node 4 (d=15 mm). What is remarkable is that the biggest tensile stresses are observed on layers located between 5 and 25 mm.

Fig.8 displays the evolution of damage spatial distribution with thermal loading time. Until time 50 s, no damage occurred in the specimen. At time 100 s no damage is still observed on the heat face whereas damage reached 0.8 at the node 2, located 5 mm far, its maximum value and then decreased with increasing distance and is cancelled at node 6 located 25 mm far. Making parallel with normal stresses spatial evolution reported previously, this indicates that damage first occurs in the zone subjected to tensile state of stress. At time 150 s, damage is present at the heated face (node 1) at moderate value (0.2) and has considerably increased to 0.9 at the node 2 located 5 mm far and then decreased and canceled at node 7 located 30 mm far: the zone subjected to damage has then widened. At time 200 s, damage has increased on the heated face and reached its maximum value of 1 at the nodes 3 to 5 located at 10, 15 and 20 mm to the heated face, respectively. For higher loading times, damage increased at the heated face (node 1), remained constant at nodes 3 to 6 located at 10, 20 and 25 mm and then decreased but increased with increasing time. Hence at time 600 s, damage at the node 9 located 40 mm to the heated face equaled 0.73. One can then make the following observations:

-This damage spatial evolution is consistent with the normal stresses spatial evolution. As the tensile zone moves inside the specimen, damage occurred and increased with increasing time.

-The significant damage first appeared inside the specimen and reached its maximum value in the zone where it first appeared.

-The heated face of the specimen was also subjected to damage but at moderate level.

According to these results, the zones were spalling should be initiated are those where damage initially occurred. In order to corroborate this assumption, one should compare the thickness of the first bursts of concrete with the distance to the heated face where damage initially occurred. The thickness of the biggest splinters that was measured after the test ranged from 5 to 12 mm, what is consistent with modelling results.

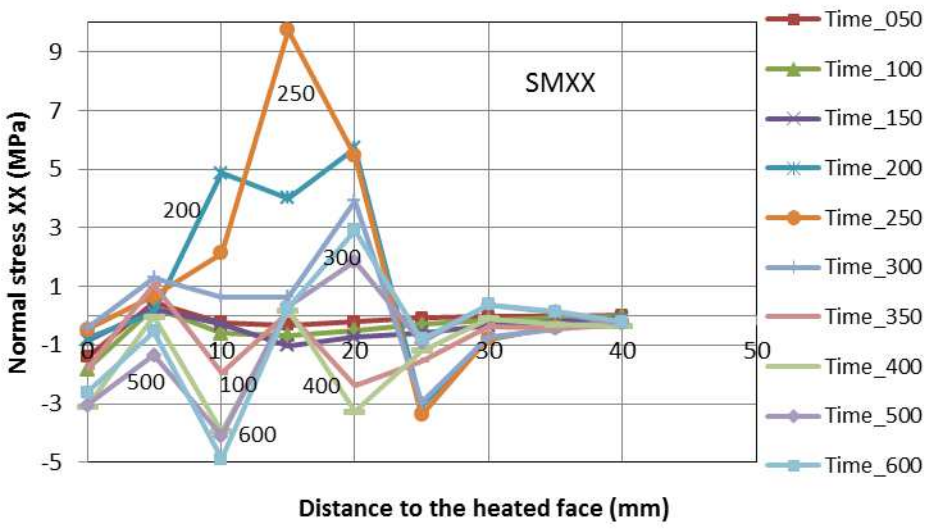

Fig.7. Evolution of the spatial distribution of X normal stresses along the specimen's height.

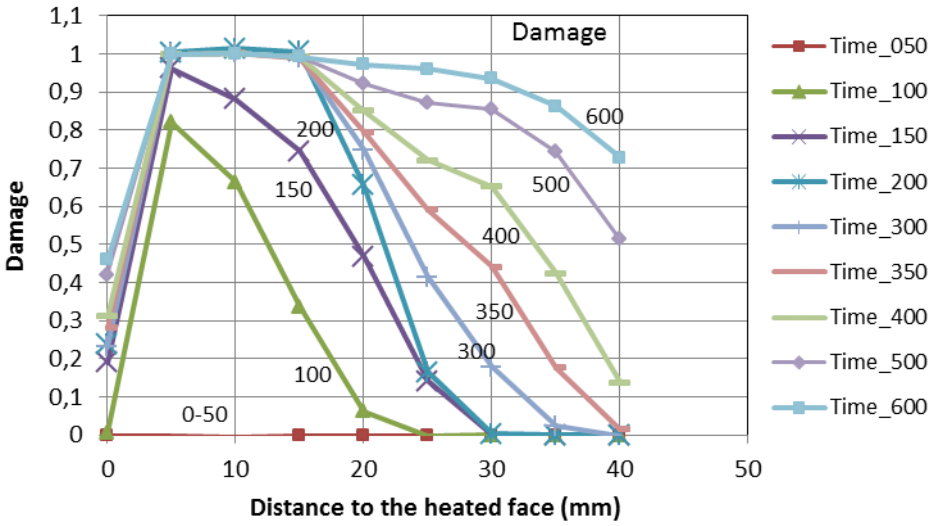

Fig.8. Evolution of the spatial distribution of damage along the specimen's height.

6 Conclusion

A spalling test was undertaken on a high performance concrete specimen equipped with three thermocouples that measured the temperature at the heated face and at two other points located at different distances. The temperature measured at the heated face was then used as an input for the finite element model to compute the temperature field in imposed–temperature conditions. Hence, the thermal numerical modelling satisfactorily predicted the temperature evolution of the thermocouples by computing the temperature evolution with respect to time at nodes of the same locations as the thermocouples. It was then possible to compute confidently stresses and damage considering an isotropic damage constitutive model. The computed damage field showed that the most damage zones were inner layers corresponding logically to the most tensile stressed zones. Hence, when spalling occurs, the thickness of the concrete bursts should be bigger than 5 mm: that is in accordance with the first experimental observations.

References

[1] C. G. Han, M. C. Han, and Y. S. Heo, Spalling properties of high strength concrete mixed with various mineral admixtures subjected to fire. Concrete Structures and Materials, 2(1):41–48, 2008.
[2] P. Kalifa, F.D. Menneteau, and D. Quenard, Spalling and pore pressure in hpc at high temperatures. Cement and Concrete Research, 30:1–13, 2000.
[3] G.A. Khoury and B. Willoughby, Polypropylene fibres in heated concrete, Part 1: molecular structure and materials behavior, Magazine of concrete research, 60(2):125– 136, 2008.
[4] P. Kalifa, G. Chéné, and C. Gallé, High temperature behaviour of hpc with polypropylene fibres: from spalling to microstructure. Cement and Concrete Research, 31(10):1487–1499, 2001.
[5] G.A. Khoury, Polypropylene fibres in heated concrete. Part 2: pressure relief mechanisms and modelling criteria. Magazine of concrete research, 60(3):189–204, 2008.
[6] J. Ožbolt, G. Periškić, M. Jelčic, and H.W. Reinhardt, Modelling of concrete exposed to high temperature. In 1st International Workshop on concrete spalling due to Fire Exposure, pages 461–469, Leipzig, 2009.
[7] Ozbolt J et al. 3D numerical analysis of reinforced concrete beams exposed to elevated temperature. Eng Struct (2013) http://dx.doi.org/10.1016/j.engstruct.2012.11.030

[8] E. Ouedraogo, S. Djaknoun, H. Bensalem, R. Bouchendouka, Experimental study of a very high performance concrete slab subjected to fire on its underside and numerical modeling of the temperature field, Submitted to Framcos 2019.
[9] J. Mazars, G. Pijaudier-Cabot G, Continuum damage theory - application to concrete, Journal of Engineering Mechanics, 1989, Vol. 115, p 345-365.
[10] S. Djaknoun, E. Ouedraogo, A. Ahmed-Benyahia, Experimental study of concrete behavior in compression and bending at elevated temperatures and constitutive modelling with an isotropic damage model. To be submitted.